

# On diamond surface properties and interactions with neurons

P. Ariano<sup>1,2</sup>, O. Budnyk<sup>1,3</sup>, S. Dalmazzo<sup>1,2</sup>, D. Lovisolo<sup>1,2</sup>, Ch. Manfredotti<sup>1,3</sup>, P. Rivolo<sup>4</sup>, and E. Vittone<sup>1,3,a</sup>

<sup>1</sup> Nanostructured Surface and Interface Excellence Centre (NIS), University of Torino, Italy

<sup>2</sup> Department of Animal and Human Biology and CNISM-CNR, University of Torino, Italy

<sup>3</sup> Department of Experimental Physics, University of Torino, Italy

<sup>4</sup> Department of Physics, Polytechnic of Torino, Italy

Received 22 April 2009 and Received in final form 10 September 2009

Published online: 11 October 2009 – © EDP Sciences / Società Italiana di Fisica / Springer-Verlag 2009

**Abstract.** In this paper we report about the role the diamond surface morphology and atomic termination plays in the survival and viability of neuronal cells, which represent an appropriate experimental model for the development of cell-based biosensors. The samples we have investigated were both CVD homoepitaxial diamond films and nanocrystalline diamond layers deposited on quartz substrates. Different surface terminations were induced through exposure to atomic hydrogen and to intense UV irradiation. GT1-7 cells, a neuronal line of hypothalamic origin, were plated directly onto the diamond surfaces without exogenous adhesion molecules, in order to correlate the surface topography and chemistry to cell growth and viability. The cell density on nanocrystalline diamonds after 48 h from plating was approximately 55% of the control on plastic dishes, whatever is the atomic termination of the surface, whereas the performances of homoepitaxial samples in terms of cell growth depend on surface termination and were significantly lower, 30%.

**PACS.** 87.17.Rt Cell adhesion and cell mechanics – 81.05.Uw Carbon, diamond, graphite – 87.85.jj Biocompatibility

## 1 Introduction

In recent years, several research activities have focused on the development of biosensors incorporating living cells to detect biologically active agents and environmental pollutants, for pharmaceutical screening and, in general, to obtain functional information about the effect of a stimulus on a living system [1]. Numerous techniques have been developed to monitor the response of the cells to external physico-chemical stimuli. One of the most effective approaches consists in the measurement of the electrical activity of cultured neurons by means of micro-electrode arrays [2] which provide a stable, non-invasive interface.

In order to combine the efficiency of the conventional micro-electrode arrays with the versatility of solid state and organic substrates, several attempts have been made in recent years with different approaches, mostly with silicon [3,4], organic [5] or carbon nanotubes [6] based devices. These surfaces are amenable to be micro- and nanopatterning [7,8], thus allowing the controlled growth of neuronal processes and establishment of neuronal networks. Other highly desirable properties for such devices are biocompatibility over long time spans and optical transparency, that will allow using fluorescent dyes for multiparametrical monitoring of the functional state of cell populations.

Diamond possesses all the characteristics to fulfil these requirements: its chemical inertness, mechanical stiffness, optical transparency from IR to UV and the possibility of functionalizing the surface at the nanoscale by hydrophobic and electrical conductive H termination or hydrophilic and electrically highly resistive O-termination, make this material ideal to develop new cell-based biosensors [9–13].

In particular, the high stiffness of diamond makes it an interesting material on which to study cellular adhesion and morphology, which have been shown to be influenced by the mechanical properties of the substrate [14]. The feasibility of a whole-cell biosensor based on diamond as an active substrate has been recently demonstrated [15], and the recording of action potentials and of optical signals generated by fluorescent probes [12] from a population of spontaneously firing neurons has been reported using an H-terminated homoepitaxial diamond surface as an optically transparent macroelectrode. Recently, Bonnauron *et al.* [16] reported on the fabrication of diamond Micro Electrode Arrays (MEAs) grown on silicon as well as on glass substrates, which opens new perspectives on opto/electronic signal detection from single cells.

Many of these studies were performed by plating cell cultures on monocrystalline or nanocrystalline diamond surfaces covered with appropriate adhesion molecules (*e.g.* laminin, poly-L-lysine) for a better neuron-electrode adhesion. However, these molecules may have some influence

<sup>a</sup> e-mail: [ettore.vittone@unito.it](mailto:ettore.vittone@unito.it)

on the electrical coupling between the diamond surface and the neuronal membrane; while cells in culture usually secrete several kinds of molecules, some widely used exogenous adhesion molecules, like laminin, are quite long and may influence the distance between the surface and the cell membrane [17].

To assess the biocompatibility of the diamond surfaces with different topography and chemistry and their suitability as transparent substrates for the growth of neuronal cells and for the monitoring of their electrical/optical activity, we report in this paper a study on cell survival and viability on nanocrystalline and homoepitaxial diamond surfaces with oxygen and hydrogen terminations; in order to better evaluate the contribution of surface topography, any protein layer to promote cell adhesion was used. The experiments were performed with GT1-7 neuronal cells, which represent an appropriate model of differentiated, electrically excitable and autorhythmic neuronal cells.

## 2 Experimental

### 2.1 Diamond samples

The experiments were carried out using three nanocrystalline (NCD) diamond films deposited on ( $1 \times 1 \text{ cm}^2$ ) quartz substrate by a modified hot-filament process (patented  $\rho$ -Best process) [18] and one homoepitaxial (OMO) IIa layer by Micro Wave Chemical Vapour Deposition (MWCVD) on a ( $3 \times 3 \times 1 \text{ mm}^3$ ) High Pressure High Temperature (HPHT) Ib diamond substrate, (100) oriented.

### 2.2 Sample preparation

#### 2.2.1 Cleaned samples

All samples were cleaned and chemically oxidized with hot sulfochromic acid at  $125^\circ\text{C}$  for 4 h, rinsed with deionised water, then with low-residues content acetone, with isopropyl alcohol and finally dried in flowing argon. This cleaning procedure leads to oxidized diamond surfaces free of impurities including carbide or graphite phases [19].

#### 2.2.2 H-terminated samples

The cleaned diamond samples were then exposed to hydrogen plasma treatment for 60 min in a hot ( $2270 \text{ K}$ ) filament CVD system (chamber pressure =  $2 \text{ kPa}$ , substrate temperature =  $970 \text{ K}$ ) in order to provide hydrogen-terminated diamond surfaces.

#### 2.2.3 UV-treated samples

The method used to oxygen-terminate the sample surfaces consisted in exposing the samples in air at room temperature to UV irradiation from a deuterium lamp (Oriel 30 W Deuterium UV Source Lamp, with usable wavelength range 160 to  $400 \text{ nm}$ ) for one or more days; samples

were kept  $2 \text{ cm}$  far from the source. This procedure [20] was adopted since it is a soft, dry and effective oxidizing method and allows a selective functionalization of the diamond surface in order to make microstructured sensors [21].

### 2.3 Sample characterization

The surface morphology of the as-deposited films was characterized using an atomic force microscope (AFM, Park System XE100) in non-contact mode. The scan size was  $4 \times 4 \mu\text{m}^2$  or  $3 \times 3 \mu\text{m}^2$  at resolution of  $256 \times 256$  pixels, with a scan rate of  $1 \text{ Hz}$ .

Figure 1a shows an AFM map and profile relevant to the OMO sample; the roughness (r.m.s.) of the surface is of the order of  $1 \text{ nm}$ , mainly due to the presence of grooves induced by the polishing process.

The surface of NCDs presents a stronger roughness; grains of various dimensions ranging from tens of nanometers up to few fractions of micrometers are clearly depicted by the AFM map and profile in Figure 1b.

Due to the important role played by the dimension of surface nanostructures in cell adhesion [22], we characterised the roughness of the surfaces through the evaluation of some of their basic geometrical features.

The surface fractal dimension  $D$  was determined using the so-called cube counting method [23] using the software package supplemented to the atomic-force microscope. In Table 1 the mean values of  $D$  and the relevant uncertainties are reported as evaluated considering at least three maps for any sample. The OMO sample shows a fractal dimension very close to 2, indicating a homogeneous surface, whereas the value of  $D$  for NCDs is remarkably higher, indicating a fractal nature of the surface.

Such conclusions are corroborated by the analysis of the vertical and spatial aspects of the roughness through the estimation of the root-mean-square ( $\sigma$ ) value of the surface points and the height–height correlation function  $H(r)$ , respectively. The latter has been evaluated along the fast scan direction (horizontal direction) through the formula

$$H(r = m \cdot d) = \frac{1}{N \cdot (N - m)} \sum_1^N \sum_1^{N-m} [h(n+m, l) - h(n, l)]^2, \quad (1)$$

where  $h(n, l)$  is the height of the surface measured by AFM at the point  $n, l$ ,  $N \times N$  is the total number of points and  $d$  the step size [24].

Figure 2 shows a plot of the  $H$  function for NCD and OMO samples. The curves have been evaluated by averaging different images in order to avoid errors due to undersampling [25].

The curve relevant to the OMO sample shows an oscillating behaviour, whose period is related to the groove separation induced by the polishing procedure.

Moreover, the different scales for NCDs and OMO are worth noticing, and the relevant values of  $\sigma$  (Tab. 1), which highlights the different roughness of the two sample surfaces.

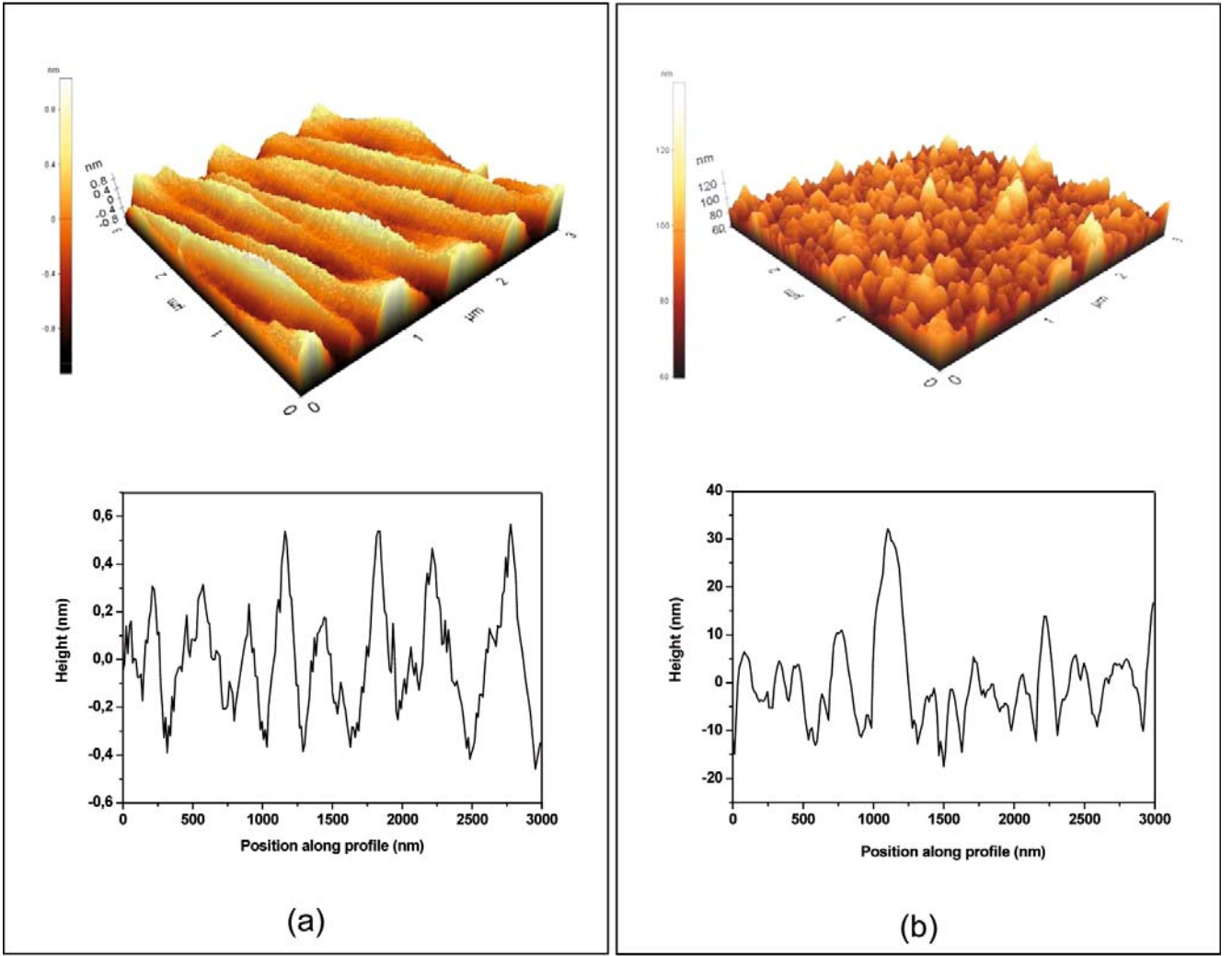


**Fig. 1.** AFM maps and profiles of the OMO (a) and NCD (b) sample surfaces.

**Table 1.** Wettability and electrical characteristics of the diamond surfaces after H or O treatments.

Sample				Termination	Water contact angle	Sheet resistivity (k $\Omega$ /sq)
NCD				Cleaned	(53.8 $\pm$ 1.3) $^\circ$	> 2 $\cdot$ 10 $^6$
$D$	$\sigma$ (nm)	$\xi$ (nm)	$\alpha$	H	(84.7 $\pm$ 0.9) $^\circ$	350 $\pm$ 200
2.28 $\pm$ 0.12	6.95 $\pm$ 0.2	91 $\pm$ 3	0.79 $\pm$ 0.06	O-UV	(48.4 $\pm$ 2.8) $^\circ$	> 2 $\cdot$ 10 $^6$
OMO				Cleaned	(53.9 $\pm$ 4.8) $^\circ$	> 2 $\cdot$ 10 $^6$
$D$	$\sigma$ (nm)			H	(76.7 $\pm$ 0.7) $^\circ$	145 $\pm$ 6
2.03 $\pm$ 0.01	0.33 $\pm$ 0.12			O-UV	(51.9 $\pm$ 0.3) $^\circ$	> 2 $\cdot$ 10 $^6$

The behaviour of the  $H$  function for NCDs is typical for a scale-invariant rough surface, which is characterized in the first linear region of the log-log plot by a slope equal to  $2 \cdot \alpha$  (*i.e.*  $H(r) \propto r^{2\alpha}$ ) and in the long-range scale, by a plateau  $H(r) = 2 \cdot \sigma^2$ .

The roughness exponent  $\alpha$  is an estimate of the random fluctuation in short range and is related to the fractal

dimension  $D$  through the following expression:

$$D = 3 - \alpha, \quad \text{with } 0 < \alpha < 1. \quad (2)$$

The turning point between the two regions is given by the correlation length  $\xi$  which represents the largest distance in which the height is still correlated. The values of the three parameters  $\sigma$ ,  $\alpha$ ,  $\xi$  completely describe the statis-

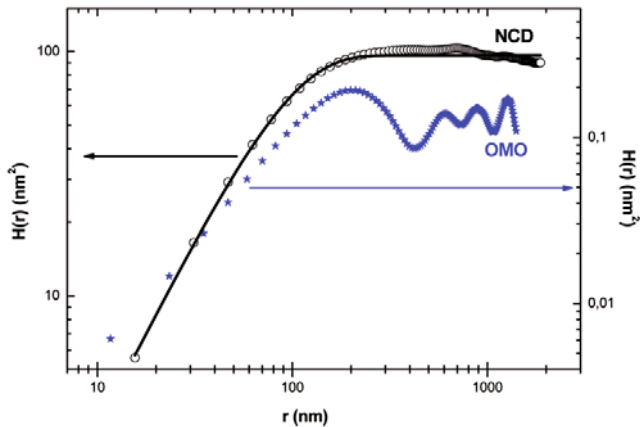


**Fig. 2.** Log-log plots of the height-height correlation function  $H(r)$  evaluated by equation (1). Circles are obtained by averaging the  $H(r)$  values AFM images scanned from 10 NCD surfaces. The continuous line is the result of the fit using equation (3). Stars: height-height correlation values for an AFM image of the OMO surface.

tical morphology of the surface within the experimental limits set by the step size of the AFM maps and can be obtained by fitting the curve of  $H(r)$  with a phenomenological scaling function of the form [26]

$$H(r) = 2 \cdot \sigma^2 \cdot \left\{ 1 - \exp \left[ - \left( \frac{r}{\xi} \right)^{2\alpha} \right] \right\}. \quad (3)$$

It is worth noticing that the value of  $\alpha$  estimated by the fitting procedure is compatible with the fractal dimension through equation (2).

Being the correlation length of the same order of magnitude as the average grain dimension, we can identify two different roughening regimes: on a subgrain scale the roughening is self-affine with roughness exponents around 0.8. Superimposed on this roughness is a grain scale effect, which causes the r.m.s. roughness.

All samples showed an optical transmittance (Fig. 3) suitable to observe cells through a standard inverted microscope and to record optical signals from fluorescent dyes. OMO samples exhibit absorption in the blue region due to the nitrogen incorporation in the Ib diamond substrate; the transmittance spectra of the NCD deposited on quartz substrate show interference patterns which allowed the estimation of the diamond layer thickness (around  $0.6 \mu\text{m}$ ) [27].

The analysis of surface composition was carried out by X-ray photoelectron spectroscopy (XPS) using Al  $K_{\alpha}$  radiation at room temperature in ultra-high vacuum utilizing a VSW class 100 spectrometer. The energy resolution of the spectrometer was about 1.2 eV.

The evaluation of the atomic percentage by XPS, related to the total analysis volume, evidenced an oxygen content of about 10% in cleaned samples. Similar results were obtained for H-terminated samples. This can be ascribed to the coverage of a thin water film, which renders the H-terminated NCD surface conductive, as described below.

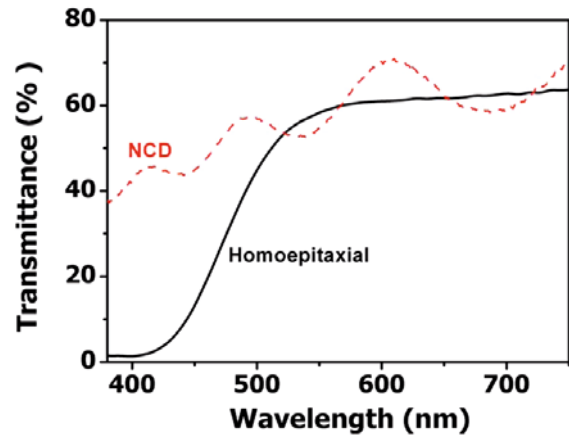


**Fig. 3.** Transmittance spectra of NCD and homoepitaxial diamond samples.

The oxygen content after UV irradiation was more than twice than after H plasma treatment. This can be ascribed both to O termination due to the decomposition of ozone by UV which partially substitutes hydrogen atoms on the surface, and to the hydrophilic character of the O-terminated surface, which favours the adsorption of water molecules from the air [20].

Measurements of wettability of the diamond surfaces were performed using the sessile drop method on a DAT-PHYSICS OCA 20 contact angle meter. A  $1 \mu\text{l}$  drop of ultrapure water was placed onto the prepared sample surface, taking at least three different measurements for each sample.

All H-terminated surfaces appear hydrophobic, with contact angles around  $80^\circ$  both for NCD and OMO samples; cleaned or UV-treated samples showed a more hydrophilic character (contact angles around  $50^\circ$ ) as summarised in Table 1.

Although it is well known that the roughness is influencing the hydrophobicity of the surface, our data relevant to contact angles of O-terminated NCD and OMO surfaces are within the experimental uncertainty. This can be ascribed to the value of the  $\sigma/\xi$  ratio for the NCD samples, which is in our case smaller than 0.1. Such a  $\sigma/\xi$  ratio determines a value of the roughness factor (*i.e.* the ratio between the NCD rough surface and a flat surface) of about 1, as evaluated using the model proposed by Nosonovsky *et al.*, for a random rough surface [28].

The difference between the values of the contact angle for H-terminated surfaces is to be ascribed to the role played by the uncontrollable environmental conditions, and in particular by the humidity, affecting the surface adsorbates [29].

After each treatment, the sheet resistivity of the diamond surfaces was evaluated through a collinear four-point probe head with tungsten carbide tips; the sheet resistances after different treatments are summarized in Table 1.

The sheet resistance of the OMO samples was of about  $150 \text{ k}\Omega/\text{sq}$ ; assuming a hole mobility of  $60 \text{ cm}^2 (\text{V s})^{-1}$  [30], the sheet hole concentration is about  $7 \cdot 10^{11} \text{ cm}^{-2}$ .

Such measurements are in agreement with the literature and are consistent with the electrochemical transfer doping model [30,31], which assumes the negative electron affinity of the H-terminated surface as an essential requirement for the surface conductivity induced by adsorbed molecules from atmospheric water vapour.

The sheet resistance values from measurements carried out on different NCD samples, after the same procedure for hydrogen termination, are more scattered, ranging from 100 to 500 k $\Omega$ /sq.

Cleaned or UV-treated samples showed a highly electrically resistive surface. This is due to the O-termination of the diamond surfaces, which induces a transformation of the electron affinity (from negative to positive), resulting in the increasing of the electrical resistivity of at least 5 orders of magnitude [20].

## 2.4 Cell culture, assessment of neuronal survival and calcium imaging

The experiments were conducted using GT1-7 cells at room temperature. The neuronal cells were grown in monolayer at 37°C in a humidified atmosphere of 5% CO<sub>2</sub>/air, in DMEM (4.5 g/l glucose) containing 2 mM glutamine, 50  $\mu$ g/ml gentamycin, supplemented with 10% FBS (Invitrogen Life Technologies, NY).

Cells were plated at a seeding density of about 50000 cells/cm<sup>2</sup> and cultured for two days on control plastic dishes (representing a common cell growth support material) and on cleaned, H-terminated and UV-treated NCD and OMO diamond surfaces without any coating with cell adhesion molecules.

Before plating, the substrates were sterilized by standard methods (washing in EDTA, collagenase and finally alcohol) and exposed to UV irradiation from a germicidal Hg lamp for 1 day. We did not observe any change in the electrical and optical features of the diamond samples after this sterilizing procedure.

Sterilization, plating and cell viability tests were performed in triplicate.

The morphology of attached cells was observed and photographed by inverted light microscope (TE200, Nikon, Japan). Cell survival was estimated by counting the cells that visually satisfied the criteria of selection for functional recordings: adhesion to the substrate, neurite extension, absence of intracellular vacuoles and of shrinking. The total number of cells was calculated by counting (with a semi-automated approach) neuronal cell bodies in  $n = 5$  selected fields ( $64 \times 10^4 \mu\text{m}^2$ ) for each sample, 24 and 48 hours after plating.

Cell viability was evaluated, 7 days after plating, by means of a live cell imaging set-up consisting of a monochromator system attached to an inverted microscope (TE2000, Nikon, Japan) with a S-Fluor 20 $\times$  objective. Images were acquired using an enhanced charge-coupled device camera. Cells were loaded for 30 min at 37°C with 0.5  $\mu$ M Fluo-3 (Molecular Probes, USA) and were transferred in a perfusion chamber (Bioprotechs, USA)

connected to a peristaltic pump. If not otherwise specified, all chemicals were purchased from Sigma, USA.

### 2.4.1 Statistical analysis

Data are expressed as mean  $\pm$ SEM. One-way analysis of variance (ANOVA) was performed to analyze datasets. *Post hoc* tests were used to determine statistically significant differences among the groups (Bonferroni test). The levels of significance are \* $p < 0.05$  and \*\* $p < 0.01$ .

## 3 Results and discussion

Figure 4 shows images at the phase contrast microscope of GT1-7 cells 48 hours after plating on control plastic dishes and on NCD and OMO diamond with either H or O-terminated surfaces. In all conditions cells adhered and survived. However, on the NCD, whatever is the atomic surface termination, neurons showed a morphology closer to that observed on plastics, whereas a non-negligible amount of dead and shrank cells was observed on OMO surfaces.

The cell density at 24 and 48 h of GT1-7 cells cultured on control plastics, NCD and OMO surfaces with different terminations are shown in Figure 5 and Figure 6.

From these data we can observe:

- 1) 24 hours after plating the cell density on H-terminated NCD was about 40% the density of the control, whereas on H-terminated OMO samples the cell density ratio (20%) is significantly lower ( $p < 0.05$ ).
- 2) After 48 hours, there was an increment of the cell population due to the proliferation; however, the difference between NCD and OMO samples was still significant ( $p < 0.01$ ).
- 3) On clean and UV-treated surfaces of NCD samples, the cell density was comparable to that observed on H-terminated surface, both at 24 h and 48 h; no significant differences were evidenced.
- 4) On clean OMO diamond surface, the cell densities after 24 and 48 h were similar to that on NCD.
- 5) UV-treated OMO sample shows a significantly smaller cell density with respect to the clean OMO sample.

Items 1) and 2) are certainly the most interesting results: previous experiments carried out with rat hippocampal neurons, chick ciliary ganglia [12] and mouse cortical neurons [13], highlighted the impairment of cell attachment on homoepitaxial hydrophobic H-terminated surfaces, in agreement with the present data relative to OMO diamond. On the other hand, in our experiments, the NCD surface topography plays a dominant role with respect to surface chemistry [32,33], as corroborated also by the fact that cell adhesion and proliferation on H-terminated NCD is similar to those measured on the same samples with clean or UV-treated surfaces, statistical analysis highlighted no significant differences.

An apparent disagreement between this result and those reported by other authors can be explained considering the different experimental conditions. In fact, the

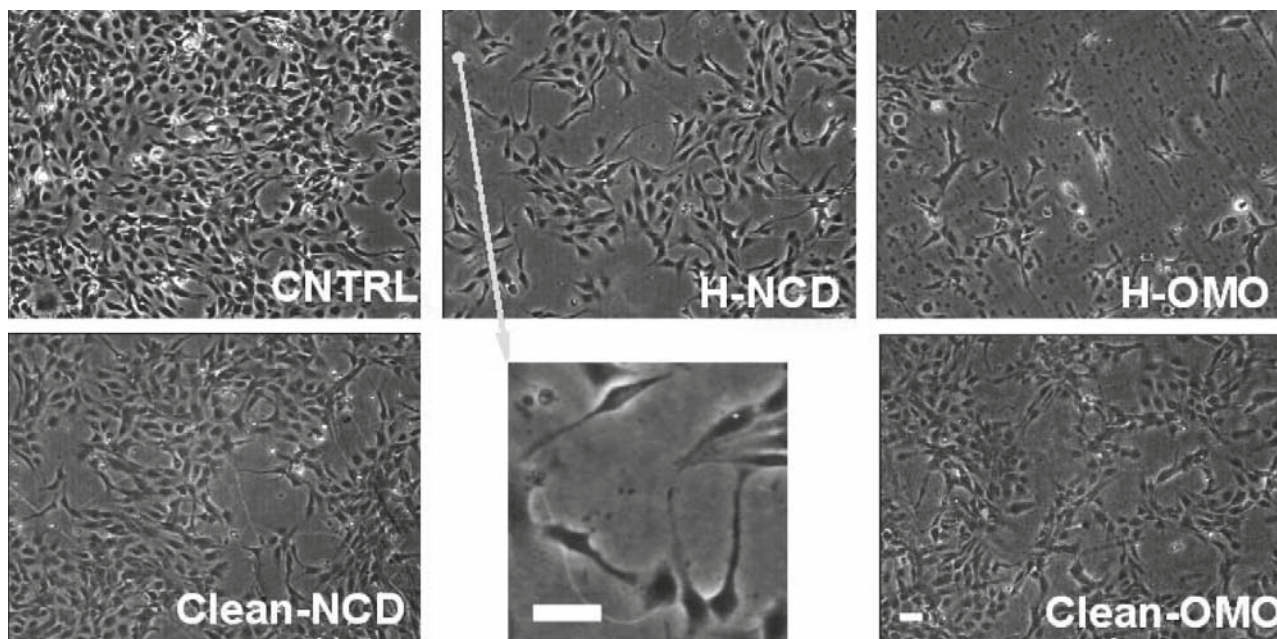


**Fig. 4.** Morphological appearance of GT1-7 cells 48 hours after plating. Upper row: on a control plastic dish, NCD and OMO diamond with H-terminated surfaces. Lower row: on a NCD and OMO diamond after the cleaning procedure. The magnified image shows in details the good morphological appearance of on H-terminated NCD. Scale bar: 50  $\mu\text{m}$ .

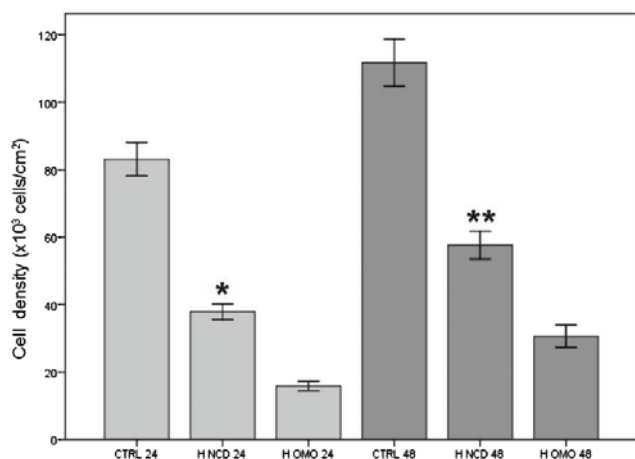


**Fig. 5.** Cell density ( $\times 10^3$  cells/cm<sup>2</sup>) at 24 and 48 hours of neurons cultured on control plastics (CTRL), NCD and OMO diamond samples with hydrogen (H) termination; \* indicates significant difference ( $p < 0.05$ ) referred to OMO 24 and \*\* indicate significant difference ( $p < 0.01$ ) versus OMO 48.

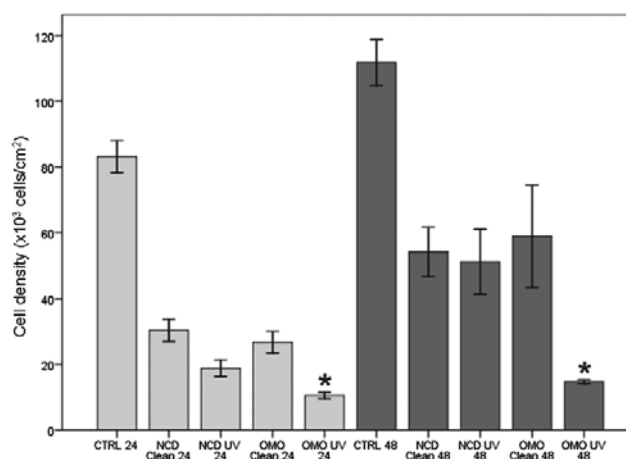


**Fig. 6.** Cell density ( $\times 10^3$  cells/cm<sup>2</sup>) at 24 and 48 hours of neurons cultured on control plastics (CTRL), NCD and OMO diamond samples with oxygen termination, clean and UV treated surfaces; \* indicates significant difference ( $p < 0.05$ ) referred to the OMO clean at the same time.

almost complete inhibition of immortalized human renal epithelial proximal tubular cells reported by Leichter *et al.* [9] was observed on H-terminated NCD diamond particles which partially covered the borosilicate glass substrate (up to 57% surface coverage) whereas, in our work, a continuous 600–800 nm thick NCD layers were used. Chong *et al.* [10] carried out adhesion experiments on NCD samples with features similar to those described in this work. However, data reported on pheochromocytoma (PC12) cells concern the attachment on H-terminated or

functionalised surfaces coated with laminin, whereas no extracellular matrix protein coatings were used in our experiment. Moreover, a direct comparison of the different adhesion behaviour on H-terminated NCD surfaces of normal human dermal fibroblast cells reported by Chong *et al.* [10] and of the GT1-7 neurons used in this work can be inappropriate, due to the different requirements for cell adhesion between the two cell lines.

It is worth emphasizing that GT1-7 neurons represent an appropriate model of differentiated, electrically

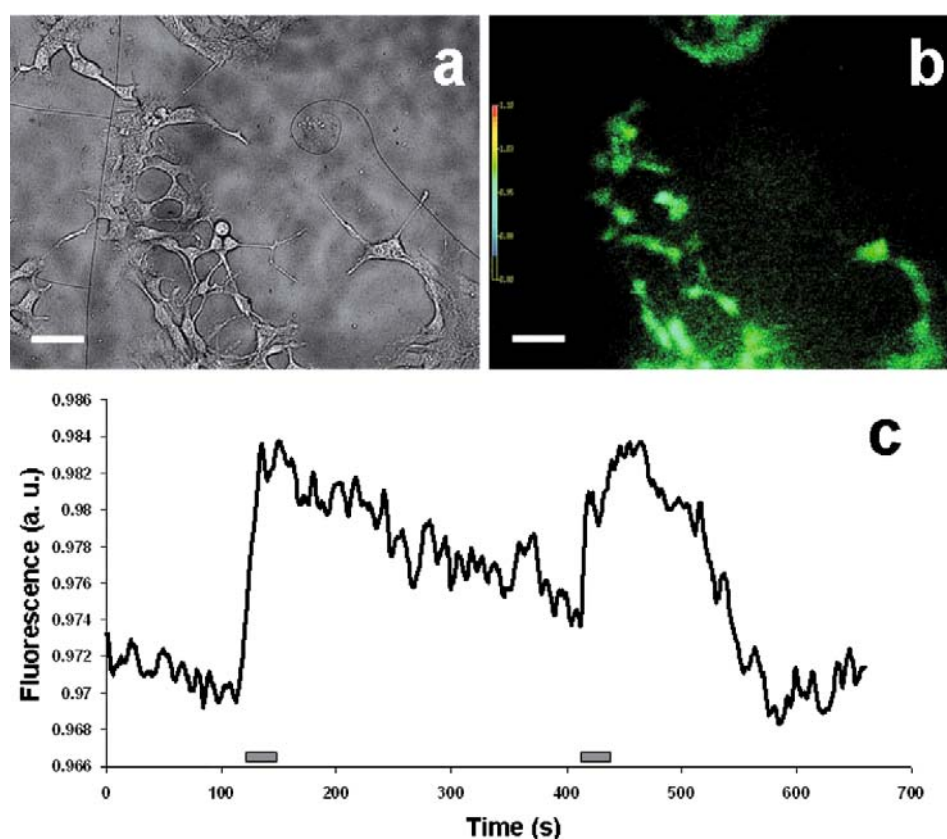


**Fig. 7.** a) Phase contrast image of GT1-7 cells cultured for 7 days on H-terminated NCD. b) Fluorimetric image of the same field of view. Scale bar: 50  $\mu\text{m}$ . c) Cytofluorimetric recordings of intracellular  $[\text{Ca}^{2+}]$ , the increase from baseline was induced by perfusion of a solution containing 40 mM KCl (grey bars at the bottom).

excitable and autorhythmic neuronal cells, whose action potential signals have been recorded by H-terminated OMO diamond electrodes covered with poly-L-lysine layer to enhance cell adhesion [15].

In the case of O-terminated surfaces, NCD clean or UV-treated surfaces showed a similar adhesion with respect to H-terminated surface. On the contrary, the cell densities for clean OMO surfaces were higher than those measured after exposure to atomic hydrogen. This can be attributed to the role played by the hydrophilic surface, which promotes cell adhesion. The UV treatment of OMO surface, contrarily, did not significantly change the results obtained with H-terminated surfaces after 24 h and seems to inhibit cell growth after 48 h.

Finally, in order to test the functional viability of GT1-7 cells, we cultured cells up to 7 days on H-terminated NCD diamond and then measured intracellular  $\text{Ca}^{2+}$  concentration changes in response to activation of voltage-gated  $\text{Ca}^{2+}$  channels. Voltage-dependent  $\text{Ca}^{2+}$  influx was activated by depolarizing the membrane potential with a solution containing 40 mM KCl, thus shifting the  $\text{K}^{+}$  equilibrium potential to more positive values. The evidence for the  $\text{Ca}^{2+}$  influx was given by cytofluorimetric recordings performed by means of fluorescence microscopy; 85% of neurons responded with reversible  $\text{Ca}^{2+}$  transients upon repeated stimulations with KCl (Fig. 7).

## 4 Conclusions

In this paper we present a study on the adhesion, growth and viability of GT1-7 neuronal cells on diamond surfaces with different topography and surface terminations. Both nanocrystalline diamond deposited on quartz and homoepitaxial diamond show a good optical transmittance, which allows the observation of cell cultures through a standard inverted microscope.

In our experiments cell were maintained in the presence of 10% FBS, and the proteins present in this medium may have been adsorbed on the surface and influence cell adhesion and survival; it must be remembered, however, that GT1-7 cells, like most neuronal models, cannot attach, survive and maintain their functional properties for several days in a simple serum-free medium; some addition, such a B27 supplement [15, 34] is in general necessary, and this procedure in turn adds to the extracellular environment proteins and other molecules of unknown nature. In the present paper, all specimens were cultured on the surfaces showing different topographies in the presence of the same extracellular medium, so that a direct comparison can be correctly performed.

Cells plated on nanocrystalline diamond samples adhere, proliferate and preserve their somatic  $\text{Ca}^{2+}$  activity, whatever the chemistry of the diamond surface (H- or O-terminated), whereas the adhesion and growth of cells on

homoepitaxial diamonds significantly depend on the surface termination (the more hydrophilic, the more biocompatible the surface is).

With respect to homoepitaxial samples, the roughness at the sub-micrometer scale allows a larger surface contact area, allowing an efficient interface with electrically excitable cells.

This result is basically consistent with the conclusions of previous studies (Fan *et al.* [35,36]), which investigated the adherence and viability of central neural cells (*substantia nigra*) on silicon wafers with different surface roughness conditions.

In those works, it was found that neural adhesion occurred on surfaces within a specific range of roughness average ( $20 < Ra < 70$  nm) without coating the surface with cell adhesion proteins. It is worth noticing that in our work the *Ra* value of NCD ( $Ra < 8$  nm) surfaces is out of this range. However, the measurement of the *Ra* parameter is not exhaustive of the morphology, since it does not take in due consideration the lateral size or the 3D features of the surface. From the analysis of our AFM images it was found that neuronal cell adhesion is promoted in NCD, whose surface morphology is the combined result of a self-affine roughening within a correlation length of about 90 nm, superimposed to an uncorrelated roughening with r.m.s. of about 7 nm; cell adhesion is much lower on flat OMO surfaces with r.m.s. smaller than 1 nm.

The data presented here show that hydrogen-terminated nanocrystalline diamond can be considered a suitable conductive substrate for the realization of optically transparent and biocompatible electrodes for the recording of electrical and optical signals from living cells and suggest that NCD can be considered a potential candidate for the development of cell-based biosensors.

This work was made possible by support from Regione Piemonte (Progetto D14 “Biosensori e interazione neuronali superfici nanostrutturate” and two years grant to P.A.).

## References

1. D.A. Stenger, G.W. Gross, E.W. Keefer, K.M. Shaffer, J.D. Andreadis, W. Ma, J.J. Pancrazio, *Trends Biotechnol.* **19**, 304 (2001).
2. W.G. Gross, B.K. Rhoades, H.M.E. Azzazy, M. Wu, *Biosensors Bioelectron.* **10**, 553 (1995).
3. P. Bonifazi, P. Fromherz, *Adv. Mater.* **14**, 1190 (2002).
4. B. Besl, P. Fromherz, *Eur. J. Neurosci.* **15**, 999 (2002).
5. E. Bystrenova, M. Jelitai, I. Tonazzini, *Adv. Funct. Mater.* **18**, 1751 (2008).
6. S.E. Moulton, A.I. Minett, G.G. Wallace, *Sensor Lett.* **3**, 183 (2005).
7. A. Ruiz, L. Buzanska, D. Gilliland, H. Rauscher, L. Sirghi, T. Sobanski, M. Zychowicz, L. Ceriotti, F. Bretagnol, S. Coecke, P. Colpo, F. Rossi, *Biomaterials* **29**, 4766 (2008).
8. M.J. Mahoney, R.R. Chen, J. Tan, W.M. Saltzman, *Biomaterials* **26**, 771 (2005).
9. T. Lechleitner, F. Klauser, T. Seppi, J. Lechner, P. Jennings, P. Perco, B. Mayer, D. Steinmuller-Nethl, J. Preiner, P. Hinterdorfer, M. Hermann, E. Bertel, K. Pfaller, W. Pfaller, *Biomaterials* **29**, 4275 (2008).
10. K.F. Chong, K.P. Loh, S.R.K. Vedula, C.T. Lim, H. Sternschulte, D. Steinmuller, F.S. Sheu, Y.L. Zhong, *Langmuir* **23**, 5621 (2007).
11. K.F. Chong, K.P. Loh, K.A.Y.P. Ting, *Analyst* **133**, 739 (2008).
12. P. Ariano, P. Baldelli, E. Carbone, A. Gilardino, A. Lo Giudice, D. Lovisolo, C. Manfredotti, M. Novara, H. Sternschulte, E. Vittone, *Diamond Relat. Mater.* **14**, 669 (2005).
13. C.G. Specht, O.A. Williams, R.B. Jackman, R. Schoepfer, *Biomaterials* **25**, 4073 (2004).
14. D.E. Discher, P. Janmey, Y.L. Wang, *Science* **310**, 1139 (2005).
15. P. Ariano, A. Lo Giudice, A. Marcantoni, E. Vittone, E. Carbone, D. Lovisolo, *Biosensors Bioelectron.* **24**, 2046 (2009).
16. M. Bonnauron, S. Saada, C. Mer, C. Gesset, O.A. Williams, L. Rousseau, E. Scorsone, P. Mailley, M. Nosladek, J.-C. Arnault, P. Bergonzo, *Phys. Status Solidi A* **205**, 2126 (2008).
17. H. Sorribas, D. Braun, L. Leder, P. Sonderegger, L. Tiefenauer, *J. Neurosci. Meth.* **104**, 133 (2001).
18.  $\rho$ -BeSt coating GmbH, Exlgasse 20a, 6020 Innsbruck, Austria.
19. H. Kawarada, *Surf. Sci. Rep.* **26**, 205 (1996).
20. G. Speranza, S. Torrenzo, L. Minati, M. Filippi, M. Castellino, Cl. Manfredotti, Ch. Manfredotti, M. Dipalo, A. Pasquarelli, E. Kohn, H. El-Hajj, E. Vittone, *Diamond Relat. Mater.* **17**, 1194 (2008).
21. T. Sakai, K.S. Song, H. Kanazawa, Y. Nakamura, H. Umezawa, M. Tachiki, H. Kawarada, *Diamond Relat. Mater.* **12**, 1971, (2003).
22. C.S. Chen, M. Mrksich, S. Huang, G.M. Whitesides, *Science* **276**, 1425 (1997).
23. C. Douketis, Z. Wang, T.L. Haslett, M. Moskovits, *Phys. Rev. B* **51**, 51 (1995).
24. D. Raoufi, A. Kiasatpour, H.R. Fallah, A.S.H. Rozatian, *Appl. Surf. Sci.* **253**, 9085 (2007).
25. H.-N. Yang, Y.-P. Zhao, A. Chan, T.-M. Lu, G.-C. Wang, *Phys. Rev. B* **56**, 4224 (1997).
26. S.K. Sinha, E.B. Sirota, S. Garoff, H.B. Stanley, *Phys. Rev. B* **38**, 2297 (1988).
27. Z.G. Hu, P. Hess, *Appl. Phys. Lett.* **89**, 081906 (2006).
28. M. Nosonovsky, B. Bhushan, *Microsyst. Technol.* **11**, 535 (2005).
29. J.J. Mareš, P. Hubík, J. Křištofik, J. Ristein, P. Strobel, L. Ley, *Diamond Relat. Mater.* **17**, 1356 (2008).
30. L. Gan, E. Baskin, C. Saguy, R. Kalish, *Phys. Rev. Lett.* **96**, 196808 (2006).
31. F. Maier, M. Riedel, B. Mantel, J. Ristein, L. Ley, *Phys. Rev. Lett.* **85**, 3472 (2000).
32. F. Johansson, P. Carlberg, N. Danielsen, L. Montelius, M. Kanje, *Biomaterials* **27**, 1251 (2006).
33. L.M.Y. Yu, N.D. Leipzig, M.S. Shoichet, *Mater. Today* **11**, 36 (2008).
34. A.J. Martinez Fuentes, L.H. Hu, L.Z. Krsmanovic, K.J. Catt, *Mol. Endocrinol.* **18**, 1808 (2004).
35. Y.W. Fan, F.Z. Cui, S.P. Hou, Q.Y. Xu, L.N. Chen, I.-S. Lee, *J. Neurosci. Meth.* **120**, 17 (2002).
36. Y.W. Fan, F.Z. Cui, S.P. Hou, Q.Y. Xu, L.N. Chen, I.-S. Lee, *Appl. Surf. Sci.* **187**, 313 (2002).